2021 IFAC SYSID
July 13-16, 2021. Padova, Italy

An LTV Approach to Identifying Nonlinear Systems - with Application to an RRR-Robot [1]

John Lataire * **Rik Pintelon** * **Tom Oomen** **

* *Dept. ELEC, Faculty of Engineering, Vrije Universiteit Brussel (e-mail:* jlataire@vub.ac.be*)*
** *Department of Mechanical Engineering, Eindhoven University of Technology, Eindhoven, The Netherlands.*

Abstract: Nonlinear systems are appearing in all engineering applications. Deriving models for these systems is important for instance for prediction and control. The goal of this paper is to estimate models of a class of nonlinear systems, from experimental data. When considering slowly varying setpoints, nonlinear systems can be approximated by linear time-varying models. That is, the nonlinear system is linearised around a trajectory of setpoints. The approach followed in this paper formulates the identification problem of a nonlinear system as an exploration through the relevant range of setpoints, which are identifiable by using tools for linear time-varying systems. This approach is demonstrated on an idealised simulation example, and on a real-life robotic application.

Keywords: Nonlinear systems, Frequency domain, Linear Time-Varying Systems, Mechatronics

1. INTRODUCTION

Developing a general framework to tackle the identification of nonlinear systems is extremely challenging. This is attested by the many references, each of which investigating a different model class or structure. Examples include NARMAX models (Billings, 2013), block-oriented models (Giri and Bai, 2010; Schoukens et al., 2015), nonlinear state-space models (Paduart et al., 2010; Schön et al., 2011) and artificial neural networks (Suykens et al., 1996). From an identification perspective, the difficulty of nonlinear systems is that, either, strong prior knowledge is required on the model structure, or the parameter space can be extremely large.

The challenge to use these nonlinear models to design effective controllers is perhaps even higher. In fact, control engineers very often fall back to control theory of linear systems, presuming that an LTI approximation of the system at hand is sufficient. An obvious drawback is that this approximation will only be valid for small excursions of the system's states around a predefined setpoint.

An intermediate approach, as proposed for instance by Casavola et al. (2003); Hanema et al. (2017) and Chapter 7 in Tóth (2010), is to linearise the system around a variable setpoint, which is assumed to be explicitly dependent on a measurable scheduling variable. That is, the nonlinear system is embedded into a Linear Parameter Varying (LPV) framework. A serious advantage over a full blown nonlinear identification approach is that widely applicable control paradigms exist for LPV systems (Packard, 1994; Apkarian et al., 1995; Rugh and Shamma, 2000; Leith and Leithead, 2000; De Caigny et al., 2012; Hoffmann and Werner, 2015; Abbas et al., 2018).

However, actual attempts to *identify* linearised models with a variable setpoint from real-life data on nonlinear systems are scarce, and very often limited to interpolations of LTI models (De Caigny et al., 2014). The latter is known as the 'local LPV modelling approach', and has the drawbacks that i) it can result in significant interpolation errors between setpoints, and that ii) it does not allow to detect the possible *dynamic* dependence of the model on the scheduling variable.

The current paper proposes a framework to describe nonlinear systems, subject to slow setpoint changes, as linear time-varying (LTV) systems. As opposed to an LPV framework, the dependence of the setpoint on a measurable scheduling variable is not imposed a priori. This lowers the required prior knowledge on the model structure, but also limits the applicability of the identified model to the same setpoint trajectories as in the identification data set. Nevertheless, the proposed approach can be seen as an intermediate step towards an LPV model, the extension to which is foreseen in future work.

The contribution of this paper is a proof-of-concept of an identification framework for nonlinear systems embedded in an LTV structure. It is applied to a simple simulation example and to measured data from an RRR-robot.
The proposed approach assumes that the system's input and its response are the sum of a large-but-slow contribution, defining the varying setpoint, and a fast-but-small contribution, which will allow the estimation of the

[1] This research was funded by the Research Foundation Flanders (FWO-Vlaanderen) and the Flemish Government (Methusalem Fund METH1). This work is part of the research programme VIDI with project number 15698, which is (partly) financed by the Netherlands Organisation for Scientific Research (NWO).

dynamics of the system. Based on this assumption, the system model can be written as a linear ordinary differential equation with time-varying coefficients, then identified by the estimator proposed in Lataire et al. (2017). An advantage of the approach is that it is formulated in such a way that a single experiment is sufficient to extract the LTV model. Also, little constraints are imposed on the trajectory of the setpoint variation (*e.g.* it is not necessarily periodic).
The price to pay to work in a linear framework is that the experimental conditions must allow for the separation of the input and output signals into large-but-slow and fast-but-small contributions.

In the remainder, Section 2 formalises the assumptions on the system and on the experimental conditions. Section 3 outlines the identification approach, which is then applied to a simulation example in Section 4 and to a real-life robotic application in Section 5. Conclusions are formulated in Section 6.

2. SYSTEM ASSUMPTION

The considered system is SISO (Single-Input Single-Output), described by a nonlinear differential equation:

$$f\left(y(t),\dots,y^{(n_a)}(t),u(t),\dots,u^{(n_b)}(t)\right)=0 \tag{1}$$

where $u(t)$ and $y(t)$ are considered to be the input and output signals of the system, $f(\bullet)$ is a nonlinear (static) function, and $\bullet^{(n)}$ denotes the nth derivative operator w.r.t. t.

Assumption 1. (Local linearisation). The nonlinear function f and the experimental conditions are such that the input and output signals can be decomposed into

$$u(t)=u_{\mathrm{L}}(t)+\tilde{u}(t) \tag{2}$$
$$y(t)=y_{\mathrm{L}}(t)+\tilde{y}(t) \tag{3}$$

such that

$$f\left(y(t),\dots,u^{(n_b)}(t)\right) \approx \sum_{n=0}^{n_a} a_n(t)\tilde{y}^{(n)}(t)-\sum_{n=0}^{n_b} b_n(t)\tilde{u}^{(n)}(t)-\tilde{f}(t) \tag{4}$$

with

$$-\tilde{f}(t)=f\left(y_{\mathrm{L}}(t),u_{\mathrm{L}}(t)\right) \tag{5}$$
$$a_n(t)=\left.\frac{\partial f}{\partial y^{(n)}}\right|_{y_{\mathrm{L}}(t),u_{\mathrm{L}}(t)} \tag{6}$$
$$-b_n(t)=\left.\frac{\partial f}{\partial u^{(n)}}\right|_{y_{\mathrm{L}}(t),u_{\mathrm{L}}(t)} \tag{7}$$

and $\tilde{f}(t)$, $a_n(t)$ and $b_n(t)$ are smooth and slow functions of time.

Assumption 1 is interpreted as a linearisation of the nonlinear function f around a smoothly varying setpoint given by $u_{\mathrm{L}}(t)$ and $y_{\mathrm{L}}(t)$. This imposes constraints on the experimental conditions and on the nonlinear function f: the excitation should consist of a slow component (possibly with large amplitude) $u_{\mathrm{L}}(t)$, and fast but small component $\tilde{u}(t)$, and f should be smooth in its arguments. This results in a slow and smooth response $y_{\mathrm{L}}(t)$, added to a fast response $\tilde{y}(t)$ of small amplitude. Note that $\tilde{f}(t)$ is prone to be small. In fact, if the large signals $(y_{\mathrm{L}}(t),u_{\mathrm{L}}(t))$ satisfy the system equation (1), then $\tilde{f}(t)=0$.

Proposition 1. (LTV model small signal). Under Assumption 1, the nonlinear system model (1) can be rewritten as a linear time-varying (LTV) system model

$$\sum_{n=0}^{n_a} a_n(t)\tilde{y}^{(n)}(t)\approx\sum_{n=0}^{n_b} b_n(t)\tilde{u}^{(n)}(t)+\tilde{f}(t) \tag{8}$$

This system model is a linear ordinary differential equation with smoothly time-varying coefficients, and an additional smooth term $\tilde{f}(t)$.

Proof. This follows immediately from (1) and (4). □

The approximation errors in (4) and (8) are proportional to the second derivatives of f, multiplied by the small signals:

$$\mathcal{O}\left\{\left.\frac{\partial^2 f}{\partial y^{(n)}\partial y^{(m)}}\right|_{y_{\mathrm{L}}(t),u_{\mathrm{L}}(t)}\left(\tilde{y}^{(n)}\tilde{y}^{(m)}\right)\right\}, \tag{9}$$
$$\mathcal{O}\left\{\left.\frac{\partial^2 f}{\partial u^{(n)}\partial u^{(m)}}\right|_{y_{\mathrm{L}}(t),u_{\mathrm{L}}(t)}\left(\tilde{u}^{(n)}\tilde{u}^{(m)}\right)\right\}, \tag{10}$$
$$\mathcal{O}\left\{\left.\frac{\partial^2 f}{\partial y^{(n)}\partial u^{(m)}}\right|_{y_{\mathrm{L}}(t),u_{\mathrm{L}}(t)}\left(\tilde{y}^{(n)}\tilde{u}^{(m)}\right)\right\}, \tag{11}$$

and, thus, decrease for smaller $\tilde{u},\tilde{y}$ and smoother f. For this setting (Assumption 1), the higher order terms are assumed to be negligible.

Note that the decompositions of the signals in (2) and (3) into a slow-large and a small-fast component requires a preprocessing step, involving a detrending procedure. As an alternative, the full signals can be used in the following proposition.

Proposition 2. (LTV model large signal). Under Assumption 1, the nonlinear system model (1) can be rewritten as a linear time-varying (LTV) system model

$$\sum_{n=0}^{n_a} a_n(t)y^{(n)}(t)\approx\sum_{n=0}^{n_b} b_n(t)u^{(n)}(t)+f_{\mathrm{L}}(t). \tag{12}$$

This system model is also a linear ordinary differential equation with smoothly time-varying coefficients. The additional term $f_{\mathrm{L}}(t)$ is given by

$$f_{\mathrm{L}}(t)=\tilde{f}(t)+\sum_{n=0}^{n_a} a_n(t)y_{\mathrm{L}}^{(n)}(t)-\sum_{n=0}^{n_b} b_n(t)u_{\mathrm{L}}^{(n)}(t), \tag{13}$$

which is smooth but not necessarily small.

Proof. By substituting (2) and (3) into (12), we obtain equation (8). □

An extension of Propositions 1 and 2 to MIMO (Multiple-Input Multiple-Output) systems (n_u inputs, n_y outputs) could be conceived, considering a *set of* n_y nonlinear differential equations, such as (1). This lies beyond the scope of this paper.

3. IDENTIFICATION APPROACH

The main contribution of this article is the proposed identification procedure, as follows.

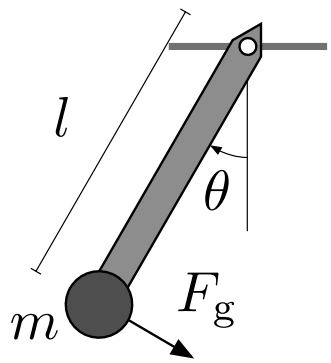

Fig. 1. Simulated pendulum, with massless stiff rod to the extremity of which a mass m is fixed, instantaneous angle θ, and F_g the component of the gravitational force mg which is perpendicular to the rod.

(1) Perform an experiment where the input signal consists of a small broad band component, with a slowly varying average, such that Assumption 1 is satisfied. This might involve a stabilising control loop if the system can be locally unstable.
(2) If Proposition 1 is used, determine $\tilde{u}(t)$ and $\tilde{y}(t)$ by detrending the signals. This will be done in the example sections by fitting smooth basis functions to the measured signals. The specific choice of the basis functions is subject to a model structure selection criterion, which can typically use prior knowledge on the applied setpoint variation.
(3) Estimate $a_n(t)$ and $b_n(t)$ by considering (8) or (12) as an LTV system. The estimator proposed in Lataire et al. (2017) will be used in Sections 4 and 5. It estimates $a_n(t)$ and $b_n(t)$ as the minimisers of a weighted least squares cost function formulated in the frequency domain, where the smoothness is imposed by including a quadratic kernel based regularisation term.

    The term $\tilde{f}(t)$ (Proposition 1) or $f_L(t)$ (Proposition 2) is dealt with by including in the model equation an additional smooth term to be estimated. Note that, the distinct terms in $f_L(t)$, as defined in (13), will not be further distinguishable.
(4) As a first step towards an LPV model identification, the dependence of the time-varying coefficients $\hat{a}_n(t)$ and $\hat{b}_n(t)$ on the setpoint variations can be visualised via scatter plots. A more formal LPV identification is foreseen for future work.

Note that Step 1 relies on the *design of an informative experiment* on the system. This includes the selection of the power spectrum of the small input signal $\tilde{u}$ to excite the dynamics of the system, and the range of the large input signal u_L to cover the domain of interest of the operating points of the system.

Also note that, in Step 3, alternative identification techniques are also useable, e.g. via a time-domain identification approach (Laurain et al., 2011) or via the use of the modulating function method (Preisig and Rippin, 1993). The method in Lataire et al. (2017) is used for its convenience of selecting the frequency band of interest and its applicability to continuous-time system.

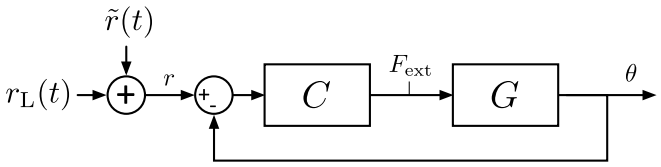

Fig. 2. Stabilising feedback configuration for the simulation example. G is the pendulum in (14), C is a PID controller, $\tilde{r}(t)$ is a small amplitude multisine signal, and $r_L(t)$ is a slowly varying angular setpoint change (ramp).

4. SIMULATION EXAMPLE

4.1 Locally linearised model

Consider the pendulum shown in Figure 1, described by the nonlinear differential equation

$$ml\theta^{(2)}(t) + \xi l\theta^{(1)}(t) + \underbrace{mg\sin\theta(t)}_{\triangleq F_g(\theta(t))} = u(t) \qquad (14)$$

with m the mass, l the length of the rod, ξ a friction coefficient, g the gravity (model parameter values in Table 1), and u an externally applied force (not shown in the figure). The force u and the angle θ are considered to be the input and the output respectively of the system. We define $\theta = 0$ as the pendulum pointing straight downwards. The component of the gravitational force perpendicular to the rod, F_g, appears as a nonlinear contribution in θ. From a first order Taylor polynomial approximation of F_g around an arbitrary θ_L:

$$F_g(\theta_L + \tilde{\theta}) \approx mg\sin\theta_L + \tilde{\theta}\underbrace{mg\cos\theta_L}_{\triangleq k(\theta_L)}, \qquad (15)$$

the pendulum equation (14) is approximated as

$$ml\theta^{(2)} + \xi l\theta^{(1)} + k(\theta_L)\tilde{\theta} \approx \tilde{u} + \tilde{f}(u_L, \theta_L) \qquad (16)$$

$$\text{with } \tilde{f}(u_L, \theta_L) = u_L - mg\sin\theta_L. \qquad (17)$$

In this expression, $\tilde{f}(u_L, \theta_L)$ can be interpreted as capturing the setpoint variation of the force, while $k(\theta_L)$ results in a restoring force with varying proportionality. Note that $k(\theta_L)$ becomes negative for $\theta_L \in]\pi/2, 3\pi/2[$ (corresponding to the upper half of the circle), possibly resulting in an *unstable* locally linearised system.

The paradigm in Proposition 1 assumes that $\theta = \theta_L + \tilde{\theta}$ where θ_L is a slow function of time and $\tilde{\theta}$ is small in amplitude such that Assumption 1 holds, resulting in the Linear Time-Varying (LTV) model in the form of (8):

$$a_2\tilde{\theta}^{(2)}(t) + a_1\tilde{\theta}^{(1)}(t) + a_0(t)\tilde{\theta}(t) = \tilde{u}(t) + \tilde{f}(t) \qquad (18)$$

For this specific case, only $a_0(t)$ is time-varying.

4.2 Simulation setup

The simulation is performed in Simulink, on the setup given in Figure 2. A feedback configuration (with C a

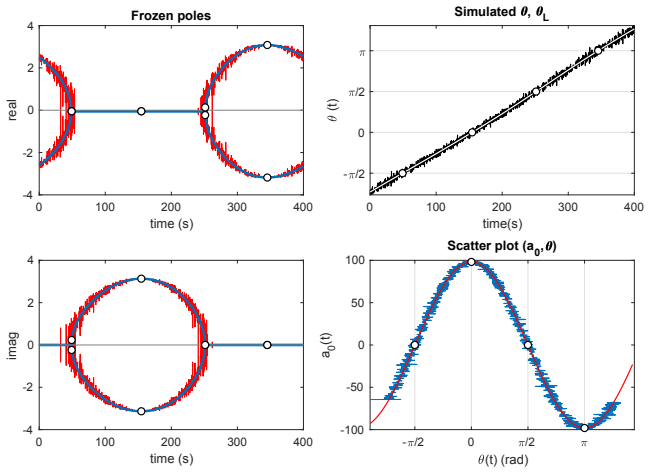

Fig. 3. Identification results on a simulation example. Left: Evolution of frozen poles (top: real part, bottom: imaginary part) (blue: estimated; red: true, locally linearised around $\theta(t)$). Top right: Simulated $\theta(t)$ (black) and trend $\theta_{\mathrm{L}}(t)$. Bottom right: blue: $(\hat{a}_0(t), \theta(t))$, red: $mg\cos(\theta)$. The black circles indicate corresponding points of interest in the four plots.

continuous time PID controller, see Table 1) is used, which ensures that the local closed loop system $G_{r\to\theta}$ is stable for all θ_{L}.

The angular reference signal is $r(t) = r_{\mathrm{L}}(t) + \tilde{r}(t)$, with

- $\tilde{r}(t)$: a zero-mean broadband (multisine) signal of small amplitude, aimed at exciting the dynamics of the system. This signal is periodic (period $T_{\mathrm{ms}} = 100\,\mathrm{s}$), excites 150 components in the band $[0.01, 4]\,\mathrm{Hz}$, and has an RMS (Root-Mean-Square) value of $\frac{\pi}{50}\,\mathrm{rad}$.
- $r_{\mathrm{L}}(t) = (\frac{2\pi}{T}t - \frac{3\pi}{4})\,\mathrm{rad}$: a slowly linearly increasing function (with $T = 4T_{\mathrm{ms}} = 400\,\mathrm{s}$ the measurement time), which establishes a scan of the range of interest of the angle.

4.3 Identification

The identification results are analysed below, on the basis of the plots in Figure 3.

- The simulated input and output are **detrended**: $u_{\mathrm{L}}(t)$ and $\theta_{\mathrm{L}}(t)$ are fitted as linear combinations of a linear function and 4 (co)sine functions to $u(t)$ and $\theta(t)$. In the top-right plot, $\theta(t)$ (black full line) and $\theta_{\mathrm{L}}(t)$ (white line) are shown. A linearly increasing trend is clearly discerned, covering the span of interest of the pendulum's angle.
- **The (time-varying) parameters of the model structure** (18) **are estimated** by providing the small signals $\tilde{u}(t) = u(t) - u_{\mathrm{L}}(t)$ and $\tilde{\theta} = \theta(t) - \theta_{\mathrm{L}}(t)$ to the KBR (Kernel Based Regression) estimator for LTV systems proposed in Lataire et al. (2017). With this estimator, the smoothness of the estimated time-varying parameters is imposed via a kernel based quadratic regularisation term, involving the Gaussian radial basis function kernel (with a length scale of 80 s), see Schölkopf and Smola (2002). Both a_0 and a_1 were allowed to be varying. Since the signals were assumed to be noiseless, the terms in the associated cost function are uniformly weighted.
- Given the estimated parameters, the **frozen transfer function** is computed as

$$\hat{G}_{\mathrm{f}}(s,t) = \frac{1}{\hat{a}_2 s^2 + \hat{a}_1(t)s + \hat{a}_0(t)}. \tag{19}$$

  This frozen transfer function can be understood as the locally linearised model around the setpoint at time instant t. Note that, although the frozen transfer function (and the frozen poles and zeroes) cannot be immediately associated with any statements on the stability of the system, they do have a one-to-one link with the time-varying differential equation such that they describe unambiguously the input-output behaviour of the system.
- In the left plots (top: real part, bottom: imaginary part), the **evolution of the frozen poles** (i.e. the poles of the frozen transfer function) are given by the blue full line. These are in good agreement with the theoretical poles (in red), obtained as the roots (in s) of the denominator of the linearised system

$$mls^2 + \xi l s + mg\cos\theta(t). \tag{20}$$

  Note that the linearised poles are computed for the raw output signal $\theta(t)$, to not be influenced by the detrending approach. This results in small excursions of the theoretical poles around the smoothed estimated poles.
- The bottom-right is a scatter plot of $(\hat{a}_0(t), \theta(t))$ (blue line), which gives a good impression of the **dependence of the restoring force on the angle**. It is in good agreement with its theoretical value $mg\cos\theta$ (red line), from (15).
- The black circles in the four plots indicate values at particular angular locations, $\theta \in \{0, \pi, \pm\pi/2\}$, corresponding to the pendulum i) pointing downwards, ii) pointing upwards, and iii) with horizontal rod. As expected, the pendulum behaves as a resonating system when pointing downwards (it has a pair of complex conjugate poles close to the imaginary axis), and has an unstable real pole when pointing upwards, i.e. for $\theta \in [\pi/2, 3\pi/2]$ in the upper half of the circle.
- The other estimated coefficients are $\hat{a}_2 = 9.9993$ and $\hat{a}_1 = 1.0009$. Their theoretical values are, respectively, $ml = 10\,\mathrm{kg.m}$ and $\xi l = 1\,\mathrm{Ns}$. Thus, a good agreement is obtained.

Table 1. Model and control parameters, simulation

G	
m	10 kg
ξ	1 Ns/m
l	1 m
g	9.81 m/s^2

C	
P	300 N/rad
I	20 N/(s.rad)
D	10 Ns/rad

It is clear that, for this simulation example, the LTV approach is able to extract the expected linearised model around the slowly varying setpoint. Of course, the current setting is close to ideal: the signals are noiseless and the model structure is known. The only errors are due to the local linearisation of the nonlinear function.

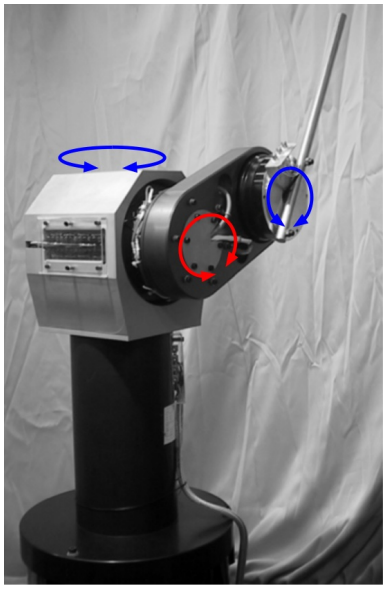

Fig. 4. RRR Robot - 3 rotational DOF robot present at the Department of Mechanical Engineering of the Technische Universiteit Eindhoven. Only the red rotational DOF is considered in this work. Picture from Kostić (2004).

5. APPLICATION TO AN RRR-ROBOT

5.1 Measurement setup

The identification approach proposed in Section 3 is applied to a 3 rotational degree-of-freedom robot (known as an RRR-robot). A complete technical description of the robot is available in van Beek (1998), and a picture is given in Figure 4. For the current work, a single degree of freedom is excited, indicated in red in the picture. This can be modelled (approximately) as a pendulum. A closed loop configuration is adopted (an unstable open loop behaviour is expected when the robot arm points upwards), with a stabilising PID controller. The voltage $u(t)$ applied to the motor and the angle $\theta(t)$ of the robot arm are considered to be the input and output signals respectively.

5.2 Identification

The results will be discussed by following the same structure as Section 4.3. One should note that, at the time of writing, the fit of the estimated model on the data

$$\text{fit} \triangleq \left(1 - \frac{\text{RMS}(\tilde{\theta} - \hat{\tilde{\theta}})}{\text{RMS}(\tilde{\theta})}\right) \tag{21}$$

is only about 50% on the estimation data set (where $\hat{\tilde{\theta}}$ is the estimated output obtained from a frequency domain simulation, for the applied input). This is also observed in the left plot of Figure 5, where $\tilde{\theta}(t)$, $\hat{\tilde{\theta}}(t)$ and $\left(\tilde{\theta}(t) - \hat{\tilde{\theta}}(t)\right)$ are shown: the difference (black) is half the size of the measured signal. Therefore, the results are preliminary and should be interpreted with some level of reservation. It is expected that treating this system as a single degree-of-freedom SISO system is too approximative. Extensions will be further considered. Nevertheless, from a qualitative

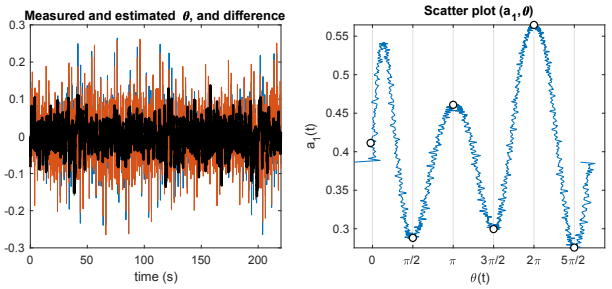

Fig. 5. Left: Measured (orange) and simulated (blue) detrended θ, and difference (black). Right: Estimated $a_1(t)$ against the measured $\theta(t)$. This gives an impression of the damping coefficient as a function of the angle.

point of view, they follow our expectations and are, thus, worthy to be discussed.

The results are discussed on the basis of the plots in Figure 6.

- A **target angle is applied**, consisting of a ramp which covers the range $[0, 2\pi]$ in 200 s, and a multisine with a period of 20 s, applied 10 times, and covering the frequency band $[0.05, 10]$ Hz.
- The measured input and output are **detrended**. The trends are fitted as linear combinations of a linear function and 6 (co)sine functions. The measured output $\theta(t)$ (in black) and its trend $\theta_{\text{L}}(t)$ (in white) are shown in the top-right plot.
- The **time-varying parameters are estimated** to the model structure given in (8) (with $n_a = 2$ and $n_b = 0$), via the detrended signals $\tilde{u}(t)$ and $\tilde{\theta}(t)$ with the KBR estimator in Lataire et al. (2017). A smoothness with a length scale of 44 s is imposed via a kernel based quadratic regularisation with a squared exponential kernel. Both a_0 and a_1 are allowed to be time-varying. The noise power spectrum is estimated by using the method in Lataire and Pintelon (2009), and used to weigh the cost function, in the format of an iterative weighted least squares, as proposed in Section 6 of Lataire et al. (2017).
- The estimated $\hat{a}_0(t)$ is plotted against the measured angle $\theta(t)$, in the bottom-right plot, and the evolution of the poles of the frozen transfer function is given in the left two plots (top: real part, bottom: imaginary part). As expected, the arm behaves like a resonator when pointing downwards, and is unstable when pointing upwards.
- The estimated coefficient $\hat{a}_1(t)$ is also varying, as observed in Figure 5, right. This indicates an angular dependence of the friction. It is approximately periodic on the angle.

6. CONCLUSION

A framework has been proposed which makes it possible to identify a nonlinear system as a linear time-varying (LTV) system, by locally linearising it around a slowly evolving setpoint. This puts constraints on the experimental conditions, involving the decomposition of the signals into i) large-and-slow, and ii) small-and-fast contributions.

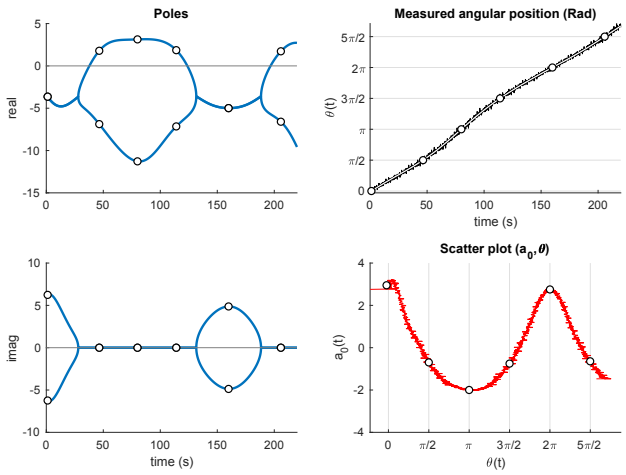

Fig. 6. Left: Time-varying pole-zero map, measurement example. Top-Right: measured angle $\theta(t)$ (black), and estimated trend $\theta_{\mathrm{L}}(t)$. Bottom-right: visualisation of the dependence of a_0 on the angle θ. The black circles on all the plots correspond to the angular positions $k\frac{\pi}{2}$, with $k = 0, 1, \ldots, 5$.

However, it allows for an identification from a single experimental data set, with little prior knowledge required on the structure of the nonlinear system. A state-of-the-art identification routine for LTV systems has been used to estimate the model, with convincing results on a simulation example and promising results on a real-life application. An extension towards LPV system is foreseen for the near future.

REFERENCES

Abbas, H.S., Hanema, J., Tóth, R., Mohammadpour, J., and Meskin, N. (2018). An improved robust model predictive control for linear parameter-varying input-output models. *International Journal of Robust and Nonlinear Control*, 28(3), 859–880.

Apkarian, P., Gahinet, P., and Becker, G. (1995). Self-scheduled $\mathcal{H}_\infty$ control of linear parameter-varying systems: a design example. *Automatica*, 31(9), 1251 – 1261.

Billings, S.A. (2013). *Nonlinear System Identification: NARMAX Methods in the Time, Frequency, and Spatio-Temporal Domains*. John Wiley & Sons, West-Sussex (UK).

Casavola, A., Famularo, D., and Franzè, G. (2003). Predictive control of constrained nonlinear systems via LPV linear embeddings. *International Journal of Robust and Nonlinear Control*, 13(3-4), 281–294.

De Caigny, J., Camino, J.F., Oliveira, R.C.L.F., Peres, P.L.D., and Swevers, J. (2012). Gain-scheduled dynamic output feedback control for discrete-time LPV systems. *International Journal of Robust and Nonlinear Control*, 22(5), 535–558.

De Caigny, J., Pintelon, R., Camino, J..F., and Swevers, J. (2014). Interpolated modeling of LPV systems. *IEEE Transactions on Control Systems Technology*, 22(6), 2232–2246.

Giri, F. and Bai, E.W. (eds.) (2010). *Block-oriented Nonlinear System Identification*. Springer-Verlag, Berlin (Germany).

Hanema, J., Tóth, R., and Lazar, M. (2017). Stabilizing non-linear MPC using linear parameter-varying representations. In *2017 IEEE 56th Annual Conference on Decision and Control (CDC)*, 3582–3587.

Hoffmann, C. and Werner, H. (2015). A survey of linear parameter-varying control applications validated by experiments or high-fidelity simulations. *IEEE Transactions on Control Systems Technology*, 23(2), 416–433.

Kostić, D. (2004). *Data-driven Robot Motion Control Design*. Ph.D. thesis, Technische Universiteit Eindhoven.

Lataire, J. and Pintelon, R. (2009). Estimating a non-parametric, colored noise model for linear, slowly time-varying systems. *IEEE Trans. on Instrumentation and Measurement*, 58(5), 1535–1545.

Lataire, J., Pintelon, R., Piga, D., and Tóth, R. (2017). Continuous-time linear time-varying system identification with a frequency-weighted kernel based estimator. *IET Control Theory & Applications*, 11(4), 457 – 465.

Laurain, V., Tóth, R., Gilson, M., and Garnier, H. (2011). Direct identification of continuous-time linear parameter-varying input/output models. *IET Control Theory & Applications*, 5(7), 878–888.

Leith, D.J. and Leithead, W.E. (2000). Survey of gain-scheduling analysis and design. *International Journal of Control*, 73(11), 1001–1025.

Packard, A. (1994). Gain scheduling via linear fractional transformations. *Systems & Control Letters*, 22(2), 79 – 92.

Paduart, J., Lauwers, L., Swevers, J., Smolders, K., Schoukens, J., and Pintelon, R. (2010). Identification of nonlinear systems using polynomial nonlinear state space models. *Automatica*, 46(4), 647 – 656.

Preisig, H. and Rippin, D. (1993). Theory and application of the modulating function method—i. review and theory of the method and theory of the spline-type modulating functions. *Computers & Chemical Engineering*, 17(1), 1 – 16. An international journal of computer applications in chemical engineering.

Rugh, W.J. and Shamma, J.S. (2000). Research on gain scheduling. *Automatica*, 36(10), 1401 – 1425.

Schölkopf, B. and Smola, A. (2002). *Learning with kernels*. Cambridge MA: MIT Press.

Schön, T.B., Wills, A., and Ninness, B. (2011). System identification of nonlinear state-space models. *Automatica*, 47(1), 39 – 49.

Schoukens, M., Marconato, A., Pintelon, R., Vandersteen, G., and Rolain, Y. (2015). Parametric identification of parallel Wiener–Hammerstein systems. *Automatica*, 51, 111 – 122.

Suykens, J., Vandewalle, J., and De Moor, B. (1996). *Artificial Neural Networks for Modeling and Control of Non-Linear Systems*. Kluwer, Boston.

Tóth, R. (2010). *Modeling and Identification of Linear Parameter-Varying Systems*, volume 403 of *Lecture Notes in Control and Information Sciences*. Springer-Verlag, Berlin Heidelberg, first edition.

van Beek, A. (1998). RRR-robot: instruction manual. DCT rapporten 1998.012, Technische Universiteit Eindhoven, Eindhoven, the Netherlands.